Applied Surface Science 480 (2019) 323–329

Contents lists available at ScienceDirect

Applied Surface Science

journal homepage: www.elsevier.com/locate/apsusc

Full length article

Pulsed laser deposition of thin carbon films on SiO_2/Si substrates

Teodor Milenov[a,*], Anna Dikovska[a], Georgi Avdeev[b], Ivalina Avramova[c], Kiril Kirilov[d], Daniela Karashanova[e], Penka Terziyska[f], Biliana Georgieva[e], Boris Arnaudov[d], Stefan Kolev[a], Evgenia Valcheva[d]

[a] "E. Djakov" Institute of Electronics, Bulgarian Academy of Sciences, 72 Tsarigradsko Chaussee Blvd, 1784 Sofia, Bulgaria
[b] "R. Kaishev" Institute of Physical Chemistry, Bulgarian Academy of Sciences, Acad. G. Bonchev Str., bl. 11, 1113 Sofia, Bulgaria
[c] Institute of General and Inorganic Chemistry, Bulgarian Academy of Sciences, Acad. G. Bonchev Street, bl. 11, 1113 Sofia, Bulgaria
[d] Faculty of Physics, University of Sofia, 5 James Bourchier Blvd., 1164 Sofia, Bulgaria
[e] Institute of Optical Materials and Technologies "Acad. Jordan Malinowski", Bulgarian Academy of Sciences, G. Bonchev Street, bl. 109, 1113 Sofia, Bulgaria
[f] Institute of Solid State Physics, Bulgarian Academy of Sciences, 72 Tsarigradsko Chaussee Blvd, 1784 Sofia, Bulgaria

ARTICLE INFO

Keywords:
Pulsed laser deposition
Thin carbon films
Graphene
Ellipsometry
TEM
Resistivity

ABSTRACT

Pulsed laser deposition (PLD) of thin carbon films on SiO_2/Si substrates was performed and the resulting films were examined by X-ray photoelectron spectroscopy, transmission electron microscopy (TEM), Raman spectroscopy and ellipsometry. The deposition process was accomplished by laser ablation with Nd:YAG laser (third harmonic $\lambda = 355$ nm, pulse width $\tau = 18$ ns and a repetition rate of 10 Hz) on 320–420 nm SiO_2/(001) Si substrates with surface area of 15×15 mm^2. The laser ablation process was carried out in two different deposition regimes: i) continuous regime with a deposition time of 15–1800 s; and (ii) pulse mode. As a target, carbon microcrystalline graphite disks (OD 15 mm, thickness 0.5 mm) were used. We established that films consisting of graphite nanoparticles/graphene grains of 5 to 30 nm thickness were deposited by the continuous PLD process while films comprising one to few-layered nano-sized graphene were deposited by pulsed PLD. Some films have low resistance ($\rho = (0.1–1.5) \times 10^{-3}$ Ω·m) and consist predominantly of sp^2 hybridized carbon with Raman spectrum, which resembles that of nano-sized graphene. Regardless of the PLD process used, we observed an interface film enriched with sp^3 hybridized carbon, which could be related to C—O, C—H and other interface bonds.

1. Introduction

Graphene is a two dimensional (2D) material that consists of fully sp^2 bonded carbon atoms packed tightly in a honeycomb lattice. Many application areas were predicted due to its promising properties [1]. There is only one reliable way of synthesizing high-quality graphene directly on a large area silicon substrate compatible with microelectronic applications: by epitaxy on SiC [2,3]. However, this method is relatively expensive as it requires the use of SiC substrates or SiC epitaxial films, high vacuum and high temperatures. On the other hand, the most commonly used methods are based on thermal and plasma-assisted chemical vapor deposition (CVD) on catalytic metallic substrates (usually copper or nickel) [4], i.e. even if the synthesized graphene is perfect, it cannot be used directly in microelectronics and must be transferred from the metal to another surface, which usually generates a large number of defects.

One of the techniques for physical vapor deposition widely applied in "bottom-up" technology is pulsed laser deposition (PLD). Originally, PLD technology was mainly used to deposit thin films with high crystallinity, accurate stoichiometry and thickness controlled up to the atomic monolayer [5]. In recent years, this method has been applied intensively for the cultivation of nanostructures with properties depending on the deposition conditions [6–8]. PLD has also been employed for growth of carbon nanostructures of different dimensions, including fullerenes, carbon nanotubes, graphite and diamond-like carbon [9,10]. The growth of graphene nano-sheets by using PLD has been reported for the first time by Cappelli et al. in 2005 [11]. The authors study the effect of substrate temperature on carbon film growth and the results showed that graphene could be produced at temperatures up to 900 °C [11]. Following this work, Scilletta et al. [12] reported that formation of graphene nano-sheets was affected not only by the substrate temperature, but also by the ambient atmosphere and that graphene nano-sheets are formed at high temperature in vacuum. Using PLD, Koh et al. [13] reported the growth of graphene with a few layers

* Corresponding author.
E-mail address: tmilenov@ie.bas.bg (T. Milenov).

https://doi.org/10.1016/j.apsusc.2019.02.220
Received 15 October 2018; Received in revised form 30 January 2019; Accepted 25 February 2019
Available online 26 February 2019
0169-4332/

on Ni/Si substrate. The growth of graphene on a Ni substrate by PLD was also reported by Wang et al. [14] who found that the number of graphene layers could be controlled by altering the laser pulses. In addition to Ni substrates, graphene was deposited on other metal substrates [15]. Recently, graphene was directly grown on a Si substrate by Qian et al. [16]. Graphene grown directly on insulating substrates was obtained using a Nd:YAG laser operating at 532 and 1064 nm [12,17–19]. The formation of graphene layers with photon energy of < 2.3 eV (corresponding to 532 nm) was explained by a photothermal mechanism that did not involve entanglement of C—C bonds. An alternative research effort has been devoted to the deposition of graphene films by using an ultraviolet pulsed laser (i.e. the photon energy higher than the C—C bond energy in highly oriented pyrolytic graphite (HOPG) without catalytic substrates [20,21].

The aim of the present study is to contribute to the creation of reliable methods for synthesizing single- to multi-layer nanosized graphene directly on SiO_2/(001) Si substrates.

2. Method and materials

We applied PLD by laser ablation (LA) of micro-crystalline graphite target in a standard on-axis configuration. The targets (OD 15 mm, 0.5 mm thickness) were made from microcrystalline graphite by hot-pressing and high temperature annealing (TUVEX Ltd. Bulgaria). We used pulsed Nd:YAG laser (third harmonic $\lambda = 355$ nm, pulse width $\tau = 18$ ns and a repetition rate of 10 Hz). The experimental conditions were $T_{substrates} = 700$ °C at pressure of 1×10^{-3} Pa. The carbon films were deposited on (001) Si coated with SiO_2 of thickness 320–420 nm. The SiO_2 films on Si substrates are obtained by oxidation of silicon in oxygen flow wetted by water vapor for 20 min on top of a dry oxygen flow for 15 min at about 1100 °C. Noting that the estimated ablation threshold is 1.5 J/cm^2, the PLD process was carried out in two different regimes of deposition: i) continuous regime with 15–1800 s deposition time at laser fluence of 5 J/cm^2; and ii) pulsed regime: we decreased the laser fluence to 2.5 J/cm^2 and varied N_a (duration of laser ablation, or equivalently, the number of light pulses). We used $N_a = 1$ or 2 s (10 to 20 light pulses, respectively) followed by a fixed time $N_b = 5$ s for relaxation of the deposited film. For $N_a = 1$ s we applied 12 pulse series (see Fig. 1) with total duration of the process $N_c = 12 \times (1 + 5)$ s = 72 s, while for $N_a = 2$ s we applied only 6 pulse series with $N_c = 6 \times (2 + 5)$s = 42 s.

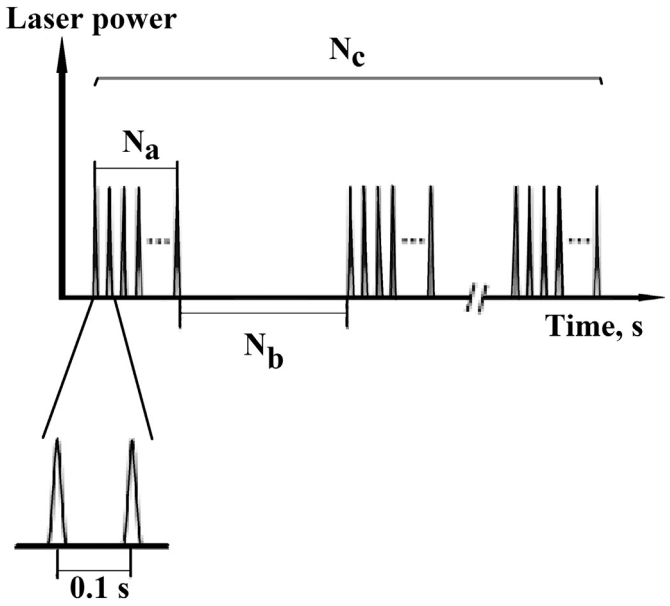

Fig. 1. The scheme of the pulsed laser ablation regime: for N_a and N_c two combinations were used: 1 s and 72 s or 2 s and 42 s, respectively, while N_b was fixed at 5 s.

After a lot of experiments conducted in continuous regime two problems remains unsolved: i) the increasing content of sp^3 hybridized carbon with decreasing thickness of the deposited film and ii) we could not deposit a continuous film with thickness below 1 nm in continuous regime. Furthermore, we established that continuous films with thickness below 1 nm could be reliably deposited in the pulsed regime, however, a residual sp^3 hybridized carbon phase of about 20% remained. In order to investigate a possible influence of the interface carbon film or the substrate, several depositions were carried out on different substrates: polished copper (10 × 10 × 0.5 mm foil, 99.999% Sigma Aldrich), 10 × 10 × 0.5 mm SS304 as well as on hydrogenated diamond-like carbon film deposited on SiO_2 (330 nm)/Si.

The XPS including Auger electron analyses were performed on a Kratos AXIS Supra spectrometer with a non-monochromatic Al X-ray source under vacuum better than 10^{-8} Pa at 90° take-off angle. Each analysis started with a survey scan from 0 to 1200 eV, pass energy of 160 eV at steps of 0.5 eV with 1 sweep. To achieve a high resolution analysis, the number of sweeps increases and passive energy decreases to 20 eV in steps of 100 meV. The C1s photoelectron line at 285 eV was used for calibration of spectra. The C1s, O1s, N1s and Si2p lines as well as CKLL Auger line were recorded for each specimen and further on, the C1s lines were subjected to additional fitting procedure with XPSPEK4.1 software.

The ellipsometry measurements were performed using Woollam M2000D rotating compensator spectroscopic ellipsometer in the wavelength range from 193 to 1000 nm. Film thicknesses and optical constants were determined by analyzing the experimental Ψ and Δ data taken at room temperature at angles of incidence 45°, 55°, 65° and 75°. The thicknesses and optical constants of the graphene (or DLC or graphite) layers and the thicknesses of the thick SiO_2 layers were determined simultaneously employing the interference enhancement method [22]. The optical constants for the SiO_2 layers and the Si substrates were taken from the Complete EASE software database. The top graphene layer was first modeled with b-spline model and afterwards converted to a General oscillator model consisting of one Cody-Lorentz oscillator and one Gaussian oscillator [23]. The top layer roughness was assumed to be zero.

The Raman spectroscopy studies were accomplished with a HORIBA Jobin Yvon Labram HR 800 spectrometer (excitation with a He—Ne (633 nm) laser). The laser beam with 0.5 mW power was focused on a spot of about 1 μm in diameter on the studied surfaces, the spectral resolution being 0.5 cm^{-1} or better. The high-resolution transmission electron microscopy (HR TEM) characterization was carried out on a HR STEM JEOL JEM 2100 microscope. The value of the accelerating voltage during TEM analysis was equal to 200 kV.

To determine the electrical resistivity of the layers the four-contact van der Pauw method as well as two-contact schemes were applied. We used indium (In) contacts (~1 mm^2) deposited on the layer surface. All contacts were distanced at least at 6 mm away from each other. The measurements were done in a dark camera using HP4140B pA-meter/dc voltage source.

3. Results and discussion

The results of the XPS study and detailed interpretation of C1s photoelectron line used for evaluation of sp^3/sp^2 ration are shown in more detail in the Supplementary materials Section. A short presentation of all deposited films (specimens C1 to C8) with description of the corresponding PLD process parameters as well as numerical results from the different characterization methods used in this work are given in Table 1.

Another simple way of using XPS to estimate the sp^3/sp^2 ratio in carbon materials is the measurement of the separation in energy of the most positive and most negative excursions of the first derivative of the carbon KLL peak, the so-called *D*-parameter — see J.C. Lascovich et al.

Table 1
Summarized data for the experimental conditions and results of the ellipsometry, XPS and electrical measurements.

Nd:YAG laser λ = 355 nm continuous regime					
Experiment	Substrate	Deposition time, s	sp^3/sp^2ratio	Thickness, nm	ρ, Ω·m
C1	SiO_2/Si	180	0.15	32.5	0.1×10^{-3}
C2	SiO_2/Si	150	0.17	26.6	
C3	SiO_2/Si	30	0.29	2.5	50×10^{-3}
C4	SiO_2/Si	600	0.15	90	

Nd:YAG laser λ = 355 nm pulsed regime							
Experiment	Substrate	N_a, s	N_b, s	N_c, s	sp^3/sp^2ratio	Thickness, nm	ρ, Ω·m
C5	Copper	2	5	49	0.19	1.2	
C6	SS304	2	5	49	0.87	1.2	
C7	aC/SiO_2/Si	2	5	49	0.44	2.5	540×10^{-3}
C8	SiO_2/Si	1	5	90	0.24	0.5	1.5×10^{-3}

[24]. This parameter is related to the width of the C KLL peak in pulse-counting form and is sensitive to the sp^3/sp^2 ratio because of the way in which the production of C KLL Auger electrons samples the structure of the valence band. The differential spectrum form (dN[E]/dE) allows evaluating the *D*-parameter — see Ref. [25], which is a measure for the abundance of sp^2 and sp^3 hybridized carbon. The D parameters of graphite and diamond are 21 eV and 13 eV, respectively.

In a recent spectroscopic study of the main carbon allotropes — S. Kaciulis et al. [26], it is pointed out that graphene is characterized by a diamond-like Auger spectrum when the spectra are excited by X-rays, whereas its Auger spectrum excited by electron beam exhibits a graphitic shape. Therefore, the proximity of our measured *D* parameter value to the one of diamond (D = 13.0 eV) implies the presence of graphene — see also Refs. [27, 28]. If the excitation is switched to the electron beam source, then this value is shifted to the graphitic one D = 21.0 eV. We obtained *D* parameters for the C5–C8 samples between 13.8 eV (for C8 specimen) and 17.5 eV (for C7 specimen) — see Fig. 2, i.e. they are typical for graphene — C8 specimen and diamond-like carbon (DLC) C6 specimen [26–28], respectively.

A detailed analysis of the ellipsometric studies of the films deposited by a continuous PLD process can be found in the work of A. Dikovska et al. [29]. Here we will focus our attention on the carbon films deposited on SiO_2/Si substrates by PLD in pulsed regime — for example the C8 specimen. The spectral dependence of the basic optical parameters of the film (the refractive index n and the extinction coefficient k) are derived from the ellipsometry measurements and are plotted in the inset of Fig. 3. The absorption coefficient (α) is calculated using the wavelength (λ) dependence of the extinction coefficient (k): $\alpha = 4\pi k / \lambda$ [30]. By means of the Tauc equation: $\alpha E = A(E - E_g)^m$, where E is the incident photon energy, E_g is the optical transition energy, m is 0.5 for the direct allowed transition and 2 for the indirect allowed transition [31], we can estimate the band gap. In Fig. 3, the obtained E_g values are plotted against photon energy, and extrapolation to lower energies of the linear portion can be used to estimate the band gap for direct transitions which shows that the band gap of C8 tends to zero.

TEM samples were prepared by dissolving the SiO_2 layer between the (001) Si substrate and the deposited film in a 15% solution of HF in doubly distilled water. The C layer removed from the substrate was several times washed in doubly distilled water, transferred onto a formvar mesh and dried. The HRTEM of specimen C3 (Fig. 4a) reveals an image typical for mixed ordered and disordered materials where in only few areas (delineated by black line as rectangles) some ordering can be detected. It is worth noting that (002) planes possessing $d_{(002)}$ = 3.4 Å [32] can be distinguished which corresponds to the observations of E. Cappelli et al. [18], i.e. the ⟨001⟩ direction is parallel to the surface in these nano-sized flakes. The HRTEM image taken from C8 (Fig. 4b) is

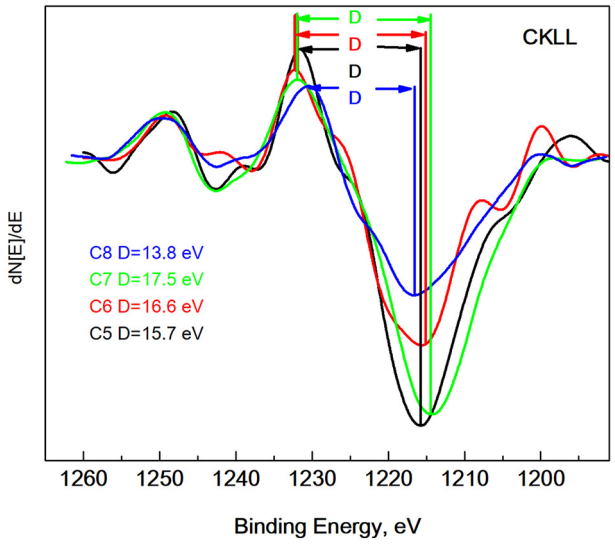

Fig. 2. Differentiated CKLL spectra after applying Savitzky-Golay algorithm excited by the X-ray source for all specimens. The determined D-parameter is 13.8 eV, 17.5 eV, 16.6 eV and 15.7 eV for specimens C8, C7, C6 and C5, respectively.

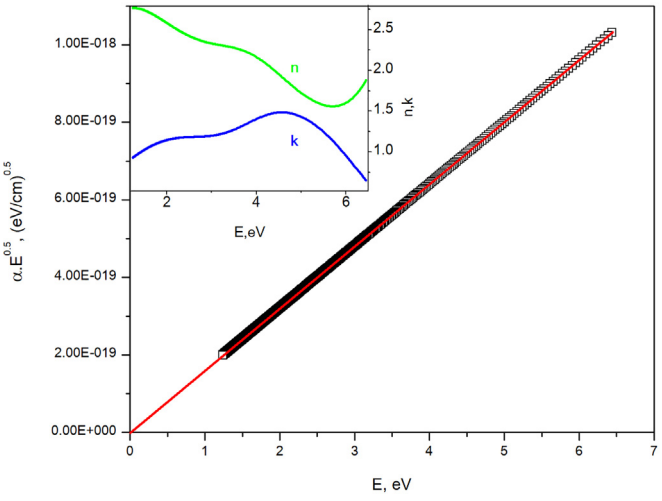

Fig. 3. Energy of the direct transition in specimen C8. The red line is a guide to the eye. The inset: plot of the spectral dependence of n and k of specimen C8. (For interpretation of the references to color in this figure legend, the reader is referred to the web version of this article.)

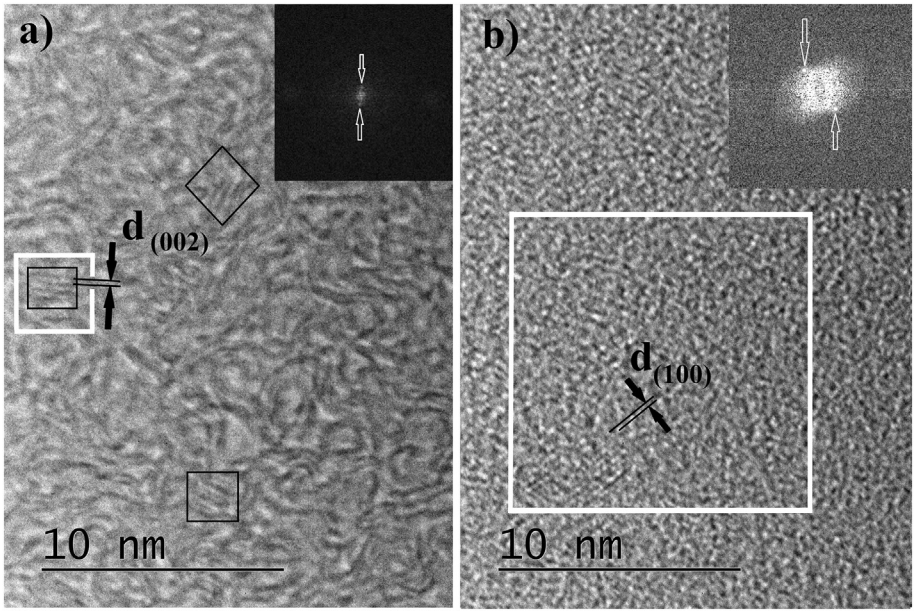

Fig. 4. HRTEM images taken from specimens C3 (a) and C8 (b). The black-line delineated rectangles in image (a) mark areas where (001) planes are clearly visible. Insets: Fast Fourier Transformation images derived from the square-shaped areas bordered by white lines.

significantly different as (100) planes with $d_{(100)}$ = 2.14 Å — Ref. [32], are visible in some areas, i.e. the ⟨001⟩ direction is perpendicular to the surface.

The Fast Fourier Transformation (FFT) images derived from the square-shaped areas bordered by white lines in Fig. 4a and b are shown in the insets of the Fig. 4a and b and clearly indicate the presence of (001) and (100) planes, respectively — the reflections are marked by white arrows. The HRTEM image of the specimen C2 is displayed in Fig. 5 a and shows lattice fringes distanced at about 5.5 Å from each other which are marked by D. The HRTEM and SAED pattern obtained from specimen C4 (thickness of 90 nm) should be related to nano-crystalline graphene — Fig. 5b. The SAED pattern (the inset of Fig.5b) reveals interplanar distances $d_{(100)}$ = 2.13 Å and $d_{(110)}$ = 1.23 Å which are typical for graphite — see Ref. [32]. The HRTEM images and SAED pattern in Figs. 4 and 5 can be used for assessment of the in-depth distribution of orientation and size of the graphene flakes. In the immediate proximity (~1 nm) to the interface the flakes lie parallel to it (Fig. 4b). At a distance of several nm from the interface the flakes orient themselves perpendicular to the surface (Fig. 4a). With increasing film thickness (20–30 nm) the flakes adopt again a planar orientation and increase in size. The HRTEM image taken from of specimen with thickness of about 30 nm in Fig. 5a reveals lattice fringes which point to flakes with significantly larger area than only several nanometers as those in Fig. 4a. With further increasing in film thickness the flakes preserve their planar orientation but with increasing disorder in the basal plane. The HRTEM and SAED pattern from C4 specimen (with thickness of 90 nm) unambiguously point to disordered graphene: the SAED pattern is typical for polycrystalline samples (see the inset of Fig. 5b). We ascribe the appearance of Fig. 5a to superimposed images of a large number of few-layered graphene flakes (due to the increased film thickness) which are misoriented to each other in the basal plane.

The Raman spectrum of perfect graphene has several strong bands: the G-band (only first order Raman feature of graphene which stems from E_{2g} phonons at Γ point of the first Brillouin zone) and 2D band (the overtone of the disorder (D) band), as well as few combination bands [33]. The D band and the additional bands: D′ and D″ arise from breathing-like modes of the carbon rings activated by defects via double-resonance Raman process [34–37]. Furthermore, the spectrum of mixed sp^2/sp^3 carbon films has two prominent features: D and G bands which appear at different wavenumbers depending on the sp^2/sp^3 ratio, sample crystallinity etc. [38]. On the other hand, the Raman spectrum of nano-sized graphene (nano-graphene) cannot be so

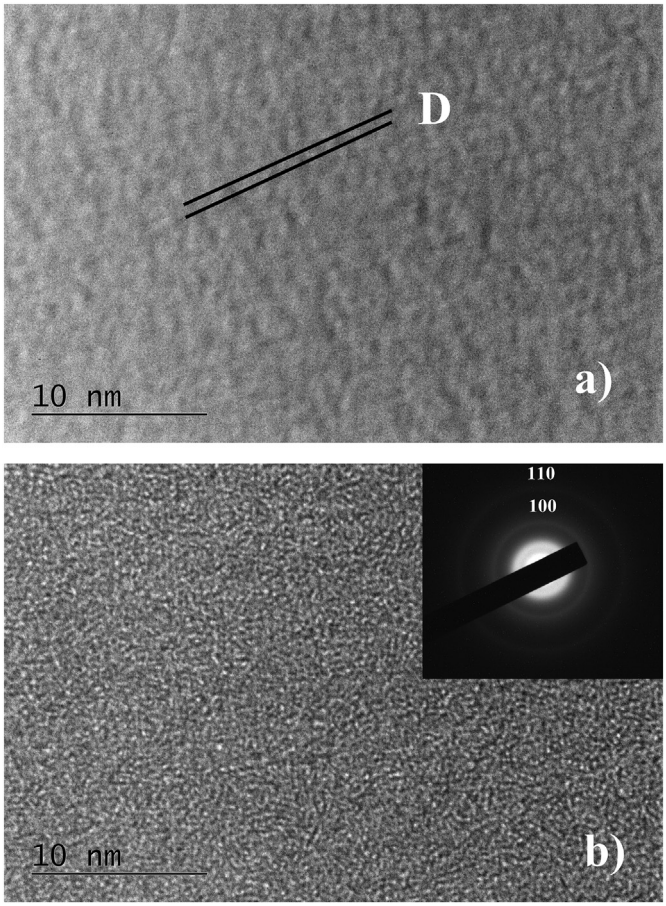

Fig. 5. a. HRTEM image taken from specimen C2. The black lines denoted two lines from lattice fringes with mean period D = 0.55 nm.
b. HRTEM image taken from specimen C4. The inset: SAED pattern taken from a specimen C4.

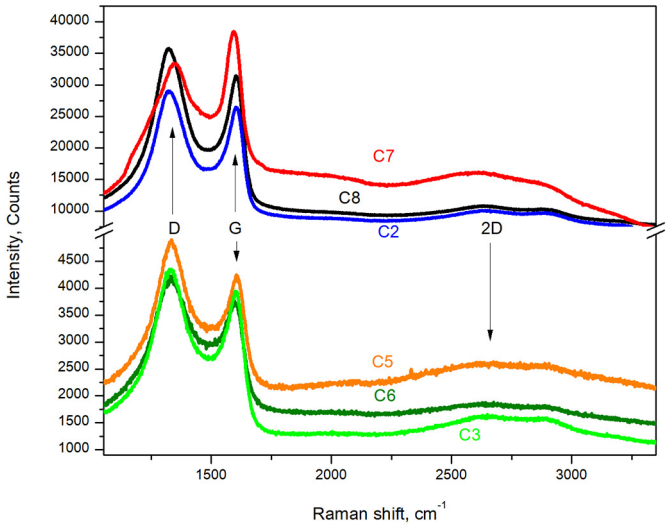

Fig. 6. Raman spectra of specimens C2, C3, C5, C6, C7 and C8. (For interpretation of the references to color in this figure, the reader is referred to the web version of this article.)

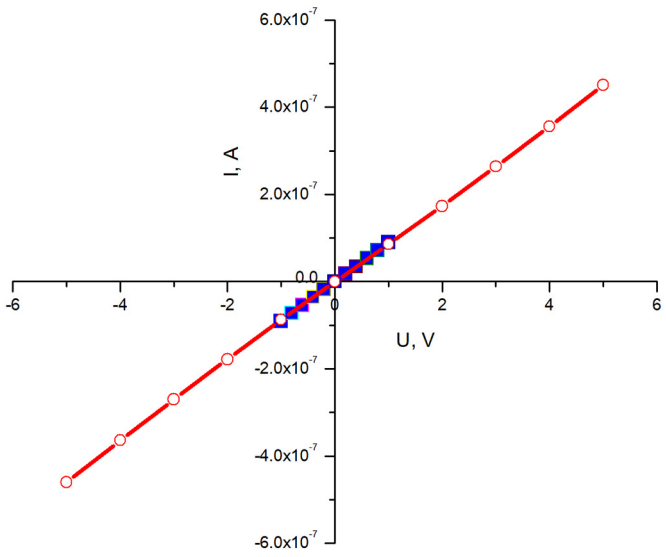

Fig. 7. I/V characteristics of the C8 specimen measured at room temperature. The measurements in the region from −0.20 to 0.20 V were repeated in a different measurement run.

definitively classified but nevertheless, few guiding lines could be derived from the spectra [39–41]: i) The D and G bands are not completely separated (even in the work of Zhang et al. [40]) and a low-intensity background or a low-intensity broadened band between D and G, centered at 1430–1450 cm^{-1} exists); ii) The G and D′ bands are more or less merged and iii) The intensity of the 2D band is 10–20% of that of the G-band.

The measured Raman spectra (Fig. 6) are complex and can be ascribed to nano-sized carbon phases possessing different phase composition (the ratio sp^2 to sp^3 hybridized carbon etc.). In order to reveal the fine differences between the main features of the experimentally obtained spectra they were deconvoluted (the deconvoluted spectrum of C8 specimen in shown in the Supplementary Materials section) and results are summarized in Table 2. Judging from the location and the band shape of the D, G and 2D bands, the Raman spectrum of specimen C8 (Table 2 and Figs. 6 and SM 3 from the Supplementary Materials section) may be regarded as a spectrum of nano-crystalline graphene. The spectrum of C2 is quite similar and the same assumption can be made by analogy — see Fig. 6. The Raman spectrum of specimens C3 and C6 (Fig. 6) can be ascribed to amorphous carbon (aC) and DLC, respectively, with a different content of sp^3/sp^2 hybridized carbon [38]. The spectrum of carbon film deposited on copper substrate — C5 (the orange trace in Fig. 6) should be similar to those of C2 and C8 but the observed worsening (the anomalously broaden bands) could be attributed to the coupling between the nano-graphene and copper substrate as shown by E. Cazzanelli et al. [42]. The Raman spectrum of C7 follows the spectrum of the substrate as shown in the Supplementary Materials section.

Table 2
Summarized data for the position and FWHM of D and G bands as well as the intensity I_G/I_{2D} ratios obtained by deconvolution of the Raman spectra of specimens from experiments C2, C3, C5, C6, C7 and C8.

Experiment	D band Position/ FWHM cm^{-1}	G band Position/ FWHM cm^{-1}	D′ band Position/ FWHM cm^{-1}	Intensity ratio I_G/I_{2D} %
C2	1323/130	1590/69	1610/53	21.7
C3	1332/150	1601/86	–/–	13
C5	1330/135	1592/71	1610/72	–/–
C6	1331/89	1585/65	1611/55	9.5
C7	1336/66	1594/74	–/–	–/–
C8	1328/126	1595/71	1612/42	14.6

Electrical resistivity measurements were carried out on specimen C1 by means of a van der Pauw circuit, while for the other higher-resistance samples the measurements were done in a two-contact circuit at DC constant voltage supply. Linear I/V dependencies were observed for all samples. This fact confirms the ohmic behavior of the samples and the contacts and allows measurement in a two-contact scheme. As expected, the aC/SiO_2/Si substrate for deposition of C7 sample has the highest resistivity and it is in the range of 10 Ω·m. The I/V characteristics of specimen C8 is shown in Fig. 7. The determined resistivity at room temperature is $\rho = 1.5 \times 10^{-3}$ Ω·m. The results for C1, C3, C7 and C8 are presented in Table 1. The resistivity of C3 is similar to that of evaporated carbon films, while that of C7 resembles the resistivity of sputtered carbon films [43]. Assuming that graphene layers typically have lower resistivity, the following analysis of the results can be made. Considering the close values of the thicknesses of the films C3 and C7 and that at the substrate of C7 there is a layer additionally enriched with sp^3-hybridized carbon, we attribute the higher resistivity of the carbon layer in specimen C7 to influence from the properties and structure of the deeper aC layer on SiO_2/Si and the interface film. Further, looking at samples C1 and C3 of differently thick carbon layers with different sp^2/sp^3 ratios deposited directly on SiO_2, it appears that the thicker carbon layer in C1 exhibits a lower resistivity, from which it can be concluded that upon increasing the layer's thickness its properties become more and more similar to those of graphene. However, an interesting observation is that the thinnest carbon layer (only 0.5 nm — specimen C8) exhibits relatively low specific resistance for the series of samples (in the order of 1×10^{-3} Ω·m), which can be taken as an indication of good deposition conditions of graphene-like layers or single to few-layered films of nano-graphene [44]. As the distance between the electric contacts was always larger than 5 mm, we consider I/V characteristics an integral sample property and can thus conclude that a reproducible deposition of single to few-layered nano-sized graphene was achieved with a resistivity similar to that of graphene with good crystalline quality. Considering that in the low-energy limit the energy of the direct optical transitions tends to 0 in both samples (see Fig. 3) [29] as determined by ellipsometry measurements, we can conclude that the films most likely consist of nano-sized graphene flakes parallel to the surface of the substrates. The HR TEM images (see Figs. 4b and 5) support such a conclusion.

According to the experimental results, several suggestions can be

deduced for continuous as well as for pulsed regimes. The deposition of carbon films in continuous regime starts with formation of local areas with amorphous structure where a significant quantity of sp^3 hybridized carbon (> 25–30%) is observed. Simultaneously, a local bonding of nano-sized few-layered graphene flakes with a ⟨001⟩ direction parallel to the substrate's surface takes place on the rest of the surface — see Fig. 3a and results of XPS study (Table 1). Further on, after deposition of such a mixed layer with thickness of 10–20 nm the deposition of nano-sized graphene flakes with ⟨001⟩ direction perpendicular to the surface occurs (see Fig. 5). The deposition of such graphene flakes is indirectly confirmed by resistivity measurements where a very low resistivity of sample C1 is established — see Table 1. The co-deposition of very small fraction of aC nanoscale regions as well as a predominantly nano-sized single- to few-layer graphene (direction [001] perpendicular to the surface of the substrate) occurs during the initial stages of the PLD in pulsed mode. Thus nano-graphene films with area of about $10 \times 10\,mm^2$ are deposited. The presence of single to few-layered graphene is confirmed directly by the C KLL Auger and Raman spectroscopy, HRTEM and indirectly by the resistivity measurements of specimen C8.

We still cannot avoid the formation of a sp^3 hybridized component on the interface substrate/carbon film — the content of sp^3 hybridized carbon in the thin film remains in the range of 15–20% even when copper substrates are used. Here it should be clearly pointed out that the ambient air even at room temperature decouples the graphene film deposited on copper by reversible oxygen intercalation and additionally, the residual atmosphere oxygen decouples graphene from copper by formation of an interface layer between the copper and graphene [45,46]. Therefore, we can ascribe the significant content of sp^3 hybridized carbon (up to 20%) to the influence of oxygen from the residual oxidation film of copper substrate and/or from the ambient atmosphere. The sp^3 fraction increases twice in the film deposited on $aC/SiO_2/Si$ substrate (C7 specimen) and four times in the films deposited on SS304 substrate (C6 specimen). The sp^3 hybridized fraction of carbon in specimen C7 is practically the same as it is in the substrate thus revealing that the main reason for its presence in C7 specimen is chemical bonding at the interface. The extremely high concentration of sp^3 hybridized carbon in specimen C6 can also be related to bonding of the carbon to oxygen (from the surface of substrate) or other the residual species.

4. Conclusions

We successfully deposited thin carbon films on SiO2/Si substrates by PLD using Nd:YAG laser (third harmonic $\lambda = 355\,nm$) at two different laser fluences (about 66% as well as about 3.3 times higher than the estimated ablation threshold) in continuous as well as in pulsed regimes. The deposited films were studied by ellipsometry, XPS (including C KLL Auger measurements), TEM, Raman spectroscopy and electrical resistivity measurements and a high process reproducibility was established. From the characterization results for the films we can conclude that: i) films consisting of nanosized few-layer graphene with a thickness of about 25–30 nm are deposited through the continuous PLD process; ii) nano-sized graphene with single to few layers is deposited by pulsed PLD; and iii) regardless of the PLD process used, we observed an interface enriched with sp^3 hybridized carbon which should be related to chemical bonding of carbon and oxygen, transition metal atoms etc. at the interface substrate/thin carbon film. The most interesting result from our point of view is the reproducible deposition of single to few-layered nano-sized graphene with a resistivity similar to that of graphene with good crystalline quality.

Acknowledgements

The authors gratefully acknowledge financial support from the Bulgarian National Science Fund under grant DN18/9-11.12.2017.

Appendix A. Supplementary data

Supplementary data to this article can be found online at https://doi.org/10.1016/j.apsusc.2019.02.220.

References

[1] K.S. Novoselov, V.I. Fal'ko, L. Colombo, P.R. Gellert, M.G. Schwab, K. Kim, A roadmap for graphene, Nature 490 (7419) (2012) 192–200.
[2] C. Berger, Z. Song, T. Li, X. Li, A.Y. Ogbazghi, R. Feng, Z. Dai, A.N. Marchenkov, E.H. Conrad, P.N. First, W.A. De Heer, Ultrathin Epitaxial Graphite: 2D Electron Gas Properties and a Route Toward, (2004), pp. 19912–19916.
[3] C. Berger, Z. Song, X. Li, X. Wu, N. Brown, C. Naud, D. Mayou, T. Li, J. Hass, A.N. Marchenkov, E.H. Conrad, P.N. First, W.A. De Heer, Electronic confinement and coherence in patterned epitaxial graphene, Science 312 (5777) (2006) 1191–1196.
[4] R. Muñoz, C. Gómez-Aleixandre, Review of CVD synthesis of graphene, Chem. Vap. Depos. 19 (10 − 12) (2013) 297–322.
[5] D. Chrisey, G. Hubler, Pulsed Laser Deposition of Thin Films, 1st ed., Wiley-Interscience, 1994.
[6] E. Fazio, F. Neri, P.M. Ossi, N. Santo, S. Trusso, Growth process of nanostructured silver films pulsed laser ablated in high-pressure inert gas, Appl. Surf. Sci. 255 (24) (2009) 9676–9679.
[7] L.M. Kukreja, S. Verma, D.A. Pathrose, B.T. Rao, Pulsed laser deposition of plasmonic-metal nanostructures, J. Phys. D. Appl. Phys. 47 (3) (2014).
[8] J. Martín-Sánchez, A. Chahboun, S.R.C. Pinto, A.G. Rolo, L. Marques, R. Serna, E.M.F. Vieira, M.M.D. Ramos, M.J.M. Gomes, A shadowed off-axis production of Ge nanoparticles in Ar gas atmosphere by pulsed laser deposition, Appl. Phys. A Mater. Sci. Process. 110 (3) (2013) 585–590.
[9] Wang, K., Tai, G., Wong, K. H., Lau, S. P. and Guo, W., "Ni induced few-layer graphene growth at low temperature by pulsed laser deposition," AIP Adv. 1(2), 0–9 (2011).
[10] Z. Yang, J. Hao, Progress in pulsed laser deposited two-dimensional layered materials for device applications, J. Mater. Chem. C 4 (38) (2016) 8859–8878.
[11] E. Cappelli, S. Iacobucci, C. Scilletta, R. Flammini, S. Orlando, G. Mattei, P. Ascarelli, F. Borgatti, A. Giglia, N. Mahne, S. Nannarone, Orientation tendency of PLD carbon films as a function of substrate temperature: a NEXAFS study, Diam. Relat. Mater. 14 (3–7) (2005) 959–964.
[12] C. Scilletta, M. Servidori, S. Orlando, E. Cappelli, L. Barba, P. Ascarelli, Influence of substrate temperature and atmosphere on nano-graphene formation and texturing of pulsed Nd:YAG laser-deposited carbon films, Appl. Surf. Sci. 252 (13 SPEC. ISS) (2006) 4877–4881.
[13] A.T.T. Koh, Y.M. Foong, D.H.C. Chua, Cooling rate and energy dependence of pulsed laser fabricated graphene on nickel at reduced temperature, Appl. Phys. Lett. 97 (11) (2010).
[14] K. Wang, Laser Based Fabrication of Graphene, 2 Intech Open, 2013, p. 64.
[15] A.E.M. Abd Elhamid, M.A. Hafez, A.M. Aboulfotouh, I.M. Azzouz, Study of graphene growth on copper foil by pulsed laser deposition at reduced temperature, J. Appl. Phys. 121 (2) (2017).
[16] M. Qian, Y.S. Zhou, Y. Gao, J.B. Park, T. Feng, S.M. Huang, Z. Sun, L. Jiang, Y.F. Lu, Formation of graphene sheets through laser exfoliation of highly ordered pyrolytic graphite, Appl. Phys. Lett. 98 (17) (2011) 12–15.
[17] I. Kumar, A. Khare, Multi- and few-layer graphene on insulating substrate via pulsed laser deposition technique, Appl. Surf. Sci. 317 (2014) 1004–1009.
[18] E. Cappelli, S. Orlando, M. Servidori, C. Scilletta, Nano-graphene structures deposited by N-IR pulsed laser ablation of graphite on Si, Appl. Surf. Sci. 254 (4) (2007) 1273–1278.
[19] E. Cappelli, S. Orlando, V. Morandi, M. Servidori, C. Scilletta, Nano-graphene growth and texturing by Nd:YAG pulsed laser ablation of graphite on silicon, J. Phys. Conf. Ser. 59 (1) (2007) 616–624.
[20] S.R. Sarath Kumar, H.N. Alshareef, Ultraviolet laser deposition of graphene thin films without catalytic layers, Appl. Phys. Lett. 102 (1) (2013).
[21] P.K. Mishra, B. Sahoo, Growth of amorphous carbon and graphene on pulse laser deposited SiC films and their characterization studies, Laser Part. Beams 31 (1) (2013) 63–71.
[22] W.A. McGahan, B. Johs, J.A. Woollam, Techniques for ellipsometric measurement of the thickness and optical constants of thin absorbing films, Thin Solid Films 234 (1–2) (1993) 443–446.
[23] CompleteEASE® Software Manual (Lincoln, USA: J. A. Woollam Co.).
[24] J.C. Lascovich, R. Giorgi, S. Scaglione, Evaluation of the sp^2/sp^3 ratio in amorphous carbon structure by XPS and XAES, Appl. Surf. Sci. 47 (1) (1991) 17–21.
[25] S. Turgeon, R.W. Paynter, On the determination of carbon sp^2/sp^3 ratios in polystyrene polyethylene copolymers by photoelectron spectroscopy, Thin Solid Films 394 (1–2) (2001) 44–48.
[26] S. Kaciulis, A. Mezzi, P. Calvani, D.M. Trucchi, Electron spectroscopy of the main allotropes of carbon, Surf. Interface Anal. 46 (10–11) (2014) 966–969.
[27] A. Mezzi, S. Kaciulis, Surface investigation of carbon films: from diamond to graphite, Surf. Interface Anal. 42 (6–7) (2010) 1082–1084.
[28] S. Kaciulis, Spectroscopy of carbon: from diamond to nitride films, Surf. Interface Anal. 44 (8) (2012) 1155–1161.
[29] A. Dikovska, L. Tzonev, I. Avramova, P. Terziiska, I. Bineva, G. Avdeev, E. Valcheva, J. Mladenoff, O. Angelov, S. Kolev, T. Milenov, Ellipsometric study of thin carbon films deposited by pulsed laser deposition, 110470N Proc. SPIE 11047, 20th International Conference and School on Quantum Electronics: Laser Physics and

Applications, 2019, https://doi.org/10.1117/12.2516970 (29 January).
[30] M.S. Dresselhaus, Solid state physics part II: optical properties of solids, Solid State Phys. (1966) 198.
[31] J. Tauc, R.V.A. Grigorovici, Optical properties and electronic structure of amorphous germanium, Phys. Status Solidi 15 (1996) 627–637.
[32] J.Y. Howe, C.J. Rawn, L.E. Jones, H. Ow, Improved crystallographic data for graphite, Powder Diffract. 18 (02) (2003) 150–154.
[33] A.C. Ferrari, J.C. Meyer, V. Scardaci, C. Casiraghi, M. Lazzeri, F. Mauri, S. Piscanec, D. Jiang, K.S. Novoselov, S. Roth, A.K. Geim, Raman spectrum of graphene and graphene layers, Phys. Rev. Lett. 97 (18) (2006) 1–4.
[34] A.C. Ferrari, D.M. Basko, Raman spectroscopy as a versatile tool for studying the properties of graphene, Nat. Nanotechnol. 8 (4) (2013) 235–246.
[35] F. Herziger, C. Tyborski, O. Ochedowski, M. Schleberger, J. Maultzsch, Double-resonant la phonon scattering in defective graphene and carbon nanotubes, Phys. Rev. B: Condens. Matter Mater. Phys. 90 (24) (2014) 1–6.
[36] C. Thomsen, S. Reich, Doable resonant Raman scattering in graphite, Phys. Rev. Lett. 85 (24) (2000) 5214–5217.
[37] L.M. Malard, M.A. Pimenta, G. Dresselhaus, M.S. Dresselhaus, Raman spectroscopy in graphene, Phys. Rep. 473 (5–6) (2009) 51–87.
[38] A.C. Ferrari, J. Robertson, Raman spectroscopy of amorphous, nanostructured, diamond-like carbon, and nanodiamond, Philos. Trans. R. Soc. A Math. Phys. Eng. Sci. 362 (1824) 2477–2512 (2004).).
[39] G. Kalita, M.S. Kayastha, H. Uchida, K. Wakita, M. Umeno, Direct growth of nanographene films by surface wave plasma chemical vapor deposition and their application in photovoltaic devices, RSC Adv. 2 (8) (2012) 3225–3230.
[40] L. Zhang, Z. Shi, Y. Wang, R. Yang, D. Shi, G. Zhang, Catalyst-free growth of nanographene films on various substrates, Nano Res. 4 (3) (2011) 315–321.
[41] M.H. Rümmeli, A. Bachmatiuk, A. Scott, F. Börrnert, J.H. Warner, V. Hoffmann, J.-H. Lin, G. Cuniberti, B. Büchner, Direct low temperature nano-graphene synthesis over a dielectric insulator, ACS Nano 4 (7) (2011) 4206–4210.
[42] E. Cazzanelli, O. De Luca, D. Vuono, A. Policicchio, M. Castriota, G. Desiderio, M.P. De Santo, A. Aloise, A. Fasanella, T. Rugiero, R.G. Agostino, Characterization of graphene grown on copper foil by chemical vapor deposition (CVD) at ambient pressure conditions, J. Raman Spectrosc. 49 (6) (2018) 1006–1014.
[43] E. Staryga, G.W. Bąk, Relation between physical structure and electrical properties of diamond-like carbon thin films, Diam. Relat. Mater. 14 (1) (2005) 23–34.
[44] I. Vlassiouk, S. Smirnov, I. Ivanov, P.F. Fulvio, S. Dai, H. Meyer, M. Chi, D. Hensley, P. Datskos, N.V. Lavrik, Electrical and thermal conductivity of low temperature CVD graphene: the effect of disorder, Nanotechnology 22 (27) (2011).
[45] P.R. Kidambi, B.C. Bayer, R. Blume, Z.J. Wang, C. Baehtz, R.S. Weatherup, M.G. Willinger, R. Schloegl, Stephan Hofmann, Observing graphene grow: catalyst-graphene interactions during scalable graphene growth on polycrystalline copper, Nano Lett. 13 (10) (2013) 4769–4778.
[46] R. Blume, P.R. Kidambi, B.C. Bayer, R.S. Weatherup, Z.-J. Wang, G. Weinberg, M.-G. Willinger, M. Greiner, S. Hofmann, A. Knop-Gerickee, R. Schlögl, The influence of intercalated oxygen on the properties of graphene on polycrystalline Cu under various environmental conditions, Phys. Chem. Chem. Phys. 16 (47) (2014) 25989–26003.